Acta Crystallographica Section A
Foundations of Crystallography
ISSN 0108-7673

Received 8 June 2004
Accepted 8 August 2004

Three exit beams from a single (*hkl*) X-ray diffraction plane

Edson M. Kakuno and Cesar Cusatis*

Universidade Federal do Parana - DF-LORXI, Brazil. Correspondence e-mail: cusatis@ufpr.br

An unusual case of three diffracted beams from a single incoming monochromatic X-ray beam and from the same Bragg plane is reported. Extremely asymmetric diffraction in a thin Si perfect crystal with a cleaved lateral face was experimentally studied. Two of the beams emerge grazing the front and back faces and the third beam emerges from the lateral face.

1. Introduction

The cases of very asymmetric diffraction in perfect crystals with the exit beam grazing the surface in coplanar geometry (Authier, 2001) were discussed theoretically by Bedynska (1973, 1974) and Härtwig (1981) and experimentally studied by Kishino (1971) and Kishino *et al.* (1972) in the Bragg and Laue geometries. An alternative theoretical analysis was given by Gramotnev (1997). In the extremely asymmetric case, it is easy to switch between Laue-case diffraction and Bragg-case diffraction and even to satisfy both cases simultaneously. From the dispersion surface (Authier, 2001) shown in Fig. 1, M is the excitation point. O and H are the centers of the dispersion surface spheres for the incident beam and diffracted beam, respectively. To′ (Th′) and To (Th) are the spheres for the vacuum and the medium, respectively. $\hat{n}$ is the line normal to the crystal surface, 1 and 2 are branch 1 and branch 2, respectively. $K_o^{(a)}$ is the incident wavevector ($2\pi/\lambda$) and its direction gives the angular direction of the incident beam, the size and position of $\overline{OH}$ are the reciprocal-lattice vector amplitude and direction, respectively. $K_o^{(d)}$ is the forward-diffracted beam.

One can see that for the grazing emergence case two beams will emerge, $K_h^{(a)}$ and $K_h^{(s)}$. One originates from tie point $P1$ (branch 1) inside the crystal, connected to the point N_s on the vacuum side on the face opposite to the incident beam, which will be called the 'Laue case' and the second beam, a traditional one, from tie point $P2$ or $P3$ (branch 2) inside the crystal, connected to the point N on the vacuum side on the same face as the incident beam, which will be called here the 'Bragg case'. Note that the angular deviation from the Laue point, La, to the actual angular position of the emergence beam (N or N_s) is one to two orders of magnitude larger than in a symmetric diffraction case owing to the curvature of the dispersion surface. The La point is given by Bragg's law,

$$\lambda = 2d \sin\theta_B. \tag{1}$$

The representation of the angular deviation, $\Delta\theta_{hc}$, in real space is show in Fig. 2. It is the correction to the angular position $2\theta_B$ for the diffracted beam.

It is possible to calculate the corrected positions of the diffracted peak grazing the front and back surfaces by using extended dynamical theory. The correction $\Delta\theta_{hc}$ for the Bragg case due to the extremely asymmetric diffraction can be calculated, as reported by Authier (2001, equation 8.8):

$$\Delta\theta_{hc} = [(\psi'^{L}_{hB})^2 + \psi'^{L}_{hB}\chi_0 \tan\theta_B - \chi_0]^{1/2} + \psi'^{L}_{hB}. \tag{2}$$

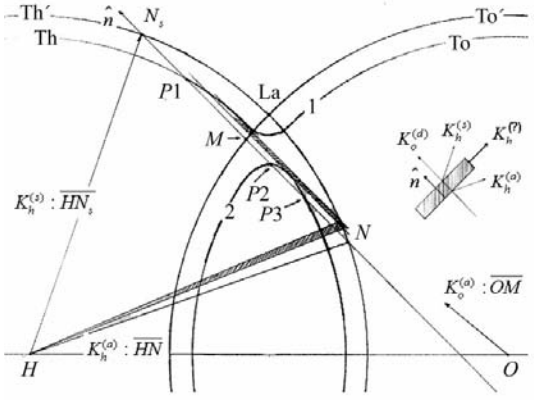

Figure 1
Dispersion surface for grazing emergence, reflection (Bragg) case.

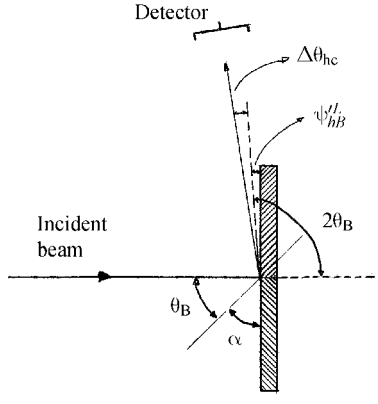

Figure 2
Correction of the diffracted-beam angular direction. Only the reflection (Bragg) geometry is represented.

A plot of this correction for Si(404) at 9131.5 eV ($\theta_B = 45^\circ$) when the asymmetry angle (α close to 45°) is changed by ψ'^{L}_{hB} is shown in Fig. 3.

For the Laue case (Authier, 2001, equation 8.9),

$$\Delta\theta_{hc} = -[(\psi'^{L}_{hB})^2 - \psi'^{L}_{hB}\chi_0 \tan\theta_B - \chi_0]^{1/2} + \psi'^{L}_{hB}. \quad (3)$$

A plot of this correction for Si(404) at 9131.5 eV ($\theta_B = 45^\circ$) when the asymmetry angle (α close to 45°) is changed by ψ'^{L}_{hB} is shown in Fig. 4.

One can see from Figs. 3 and 4 that the correction converges to zero when the diffracted beam moves away from the surface ($-\psi'^{L}_{hB}$ increases). The correction, $\Delta\theta_{hc}$, for the Laue case (Fig. 4) is negative because the positive direction of the angles is counter-clockwise. In Fig. 2, $\Delta\theta_{hc}$, the angle between the $2\theta_B$ angular direction, given by Bragg's law and the middle of the actual reflected beam profile is shown; ψ'^{L}_{hB} is the angle between $2\theta_B$ angular direction and the exit surface and is negative for the Bragg case; χ_0 is the susceptibility.

The angular width, $2\delta_{hc}$, of the diffracted beam is smaller than predicted by the standard dynamical theory. The correction of the angular width, owing to the asymmetry, in the case of an extremely asymmetric diffracted beam, diverges if the standard dynamic theory is applied. Instead, if the extended theory is used, the calculated finite width is, after Authier (2001, equation 8.14),

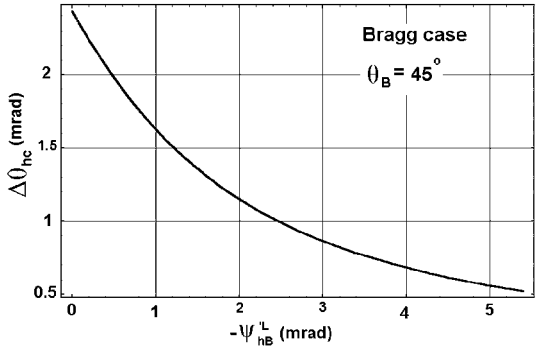

Figure 3
Angular correction of the grazing diffracted beam as a function of the equivalent grazing angle. Si(404) at 9131.5 eV.

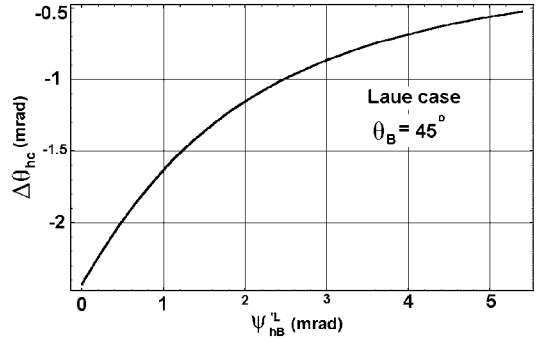

Figure 4
Angular correction of the grazing diffracted beam as a function of the equivalent grazing angle. Si(404) at 9131.5 eV.

$$2\delta_{hc} = \frac{2\delta_o[|\gamma|^{-1}]^{1/2}|\psi'^{L}_{hB}|}{[(\psi'^{L}_{hB})^2 - \psi'^{L}_{hB}\chi_0 \tan\theta_B - \chi_0]^{1/2}}. \quad (4)$$

A plot of the corrected diffracted width for Si(404) at 9131.5 eV ($\theta_B = 45^\circ$) as a function of the asymmetry angle (α close to 45°), by varying ψ'^{L}_{hB}, is shown in Fig. 5.

Note that the angular width of the diffracted beam has a maximum when the angle of the emergence beam with the surface of the crystal is near θ_C, the critical angle. $2\delta_o$ is the Darwin width calculated with the standard theory for the symmetric case and

$$\gamma = \frac{\gamma_h}{\gamma_o} = \frac{\sin(\psi'^{L}_{hB})}{\sin(2\theta_B + \psi'^{L}_{hB})} \quad (5)$$

is the asymmetry ratio.

In all these cases, the assumption is that the crystal is semi-infinite or limited in thickness without any considerations about lateral faces. In our experiment, we detected a diffracted beam emerging from the lateral face, $K_h^{(?)}$ (Fig. 1), a case not discussed in the literature. The experimental analysis of the diffracted beams from the front face, lateral face and back face is reported here and a graphic model is proposed for the beam emerging from the lateral face. These three beams were diffracting simultaneously.

2. Experimental

The experiments were carried out at the XD2 and XPD beamlines of LNLS, Brazilian Synchrotron Light Source (Laboratório Nacional de Luz Sincrotron, Campinas, Brazil). The two beamlines have the same optics with a six-circle Huber diffractometer. They are equivalent for the experiment and the use of both beamlines was necessary owing to schedule restrictions at the time of the experiments. The temperature in the experimental hall was 297±1 K. The sample, a silicon wafer consisting of a 75 µm thick perfect crystal, each lateral limited by a cleaved face perpendicular to the sample direction [100], was mounted on the six-circle goniometer. The energy was 9131.6 eV and the diffraction planes that were used, (404) and, alternatively, ($\bar{4}$04), were at 45° to the beam entrance surface, here described as 'front face'. The geometry and energy were such that the incident

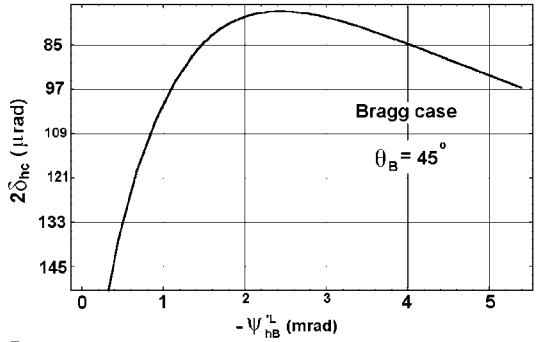

Figure 5
Corrected diffraction profile width for the grazing emergence beam, Si(404) at 9131.5 eV.

beam was normal to the wafer surface with Bragg angle (θ_B) equal to 45° and $2\theta_B$ equal to 90°, *i.e.* the exit beam grazing the surface, as shown in Fig. 6.

The 0.5 × 0.5 mm incident beam was conditioned by a mirror to minimize the vertical divergence and followed by an Si(111) double-bounce crystal monochromator with sagital focusing (Giles *et al.*, 2003). The beam was positioned at a distance of 0.75 mm from the lateral face. The 2θ scan showed three peaks, as seen in Fig. 7. This scan was done using a crystal analyzer instead of a slit. At the lower 2θ angle, we identified the first peak as Laue case, the diffracted beam emerging from the back face. The second beam came from the lateral wall (perpendicular to the front face) and is a transition between Laue and Bragg cases, and a third one was identified as Bragg case, the diffracted beam emerging from the front face. The intensity of the second beam (the extra one) increases if the incident beam is closer to the edge (lateral face) and almost disappears if the incident beam is far from the edge.

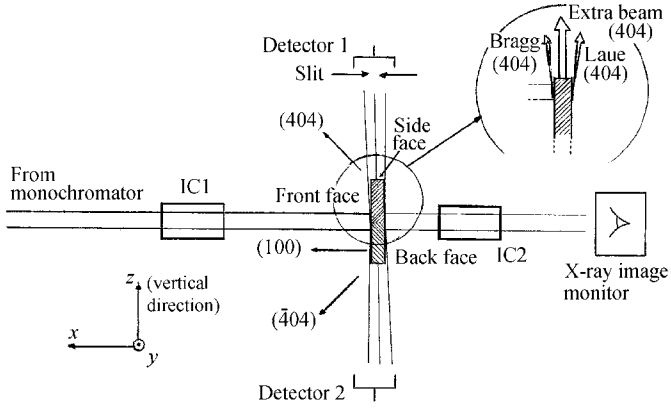

Figure 6
Experimental set-up at XD2 and XPD beamlines, LNLS.

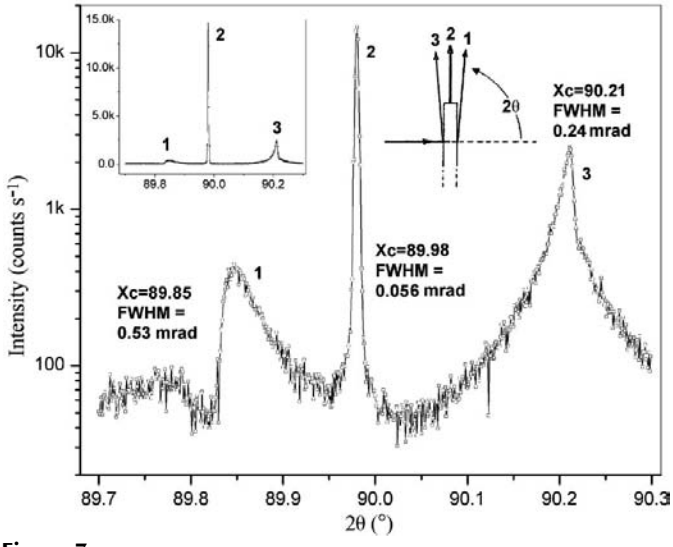

Figure 7
2θ scan with $(+n, -n)$ Si(440) analyzer. The sample is diffracting Si(404) at 9131.6 eV and $\theta_B = 45°$.

3. Determination of the energy

In the case of extremely asymmetric diffraction, it is important to know the energy with accuracy because it will define the theoretical emergence Bragg angle (point La in Fig. 1) of the diffracted beam, that is, very close and out of the surface. This is a parameter for calculating a necessary angular correction due to dynamical effects of the grazing emergence beams.

The energy of the photons delivered by the beamline monochromator has an inaccuracy of 1 eV at least, due to the standard energy calibration procedure using the energy of absorption edges.

To measure accurately the energy delivered by the monochromator, a θ scan was done with simultaneous detection (Pacherová, 1994) of the beam diffracted by Si(404) in the up direction and Si(4̄04) in the down direction, z axis in Fig. 6. The results of such scans are shown in Fig. 8.

The middle point between the (404) and the (4̄04) peaks is exactly 45° between the incident beam and the (404) Bragg planes. The distance from the middle point and the (404) peak angular position, plus 45°, is the exact Bragg angle (θ_B) for the incident wavelength. Knowing that the lattice parameter of silicon is a_{si} = 0.543102 nm at 295.6 K (Basile *et al.*, 1995; Mohr & Taylor, 2000) with the coefficient of thermal expansion $\alpha_T = 2.56 \times 10^{-6}$ K^{-1} at 295.6 K, one can compute the d_{hkl} of the

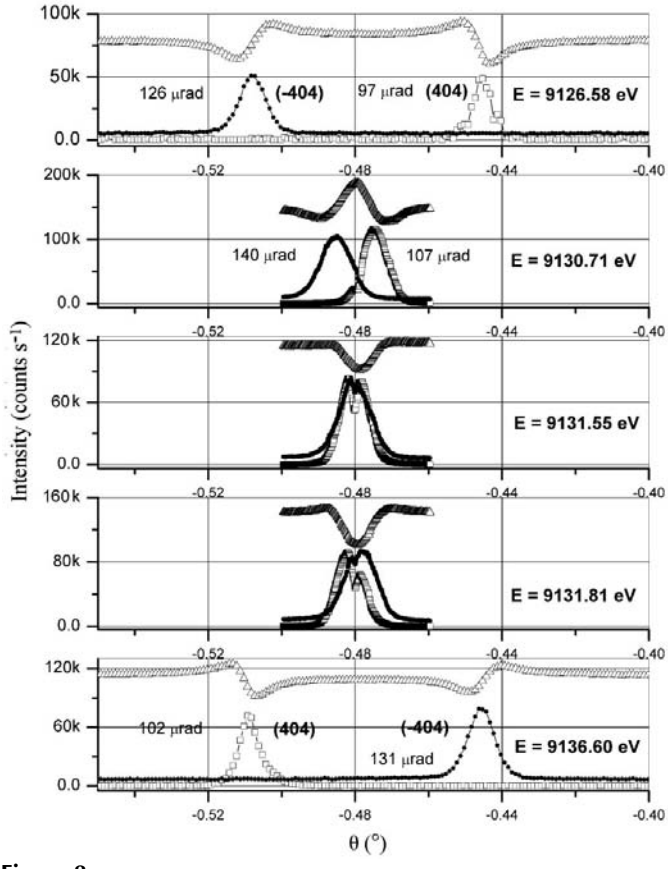

Figure 8
θ scan of the sample for energy calibration: triangles show the transmitted beam, squares show the 404 diffracted beam and the small black dots show the 4̄04 diffracted beam.

Table 1
Analysis of the Si(404) diffracted beams using an Si(440) and an Si(220) crystal analyzer in a parallel arrangement.

The bottom row shows results obtained with a 50 μm slit. The identification of the columns follows the convention adopted for Figs. 7 and 9.

Analyzer/position	(1) Laue (FWHM)	(2) Center (FWHM)	(3) Bragg (FWHM)	Direct (FWHM)
Si(440)	0.53 mrad	20 μrad	0.23 mrad	63 μrad
Si(220)	0.45 mrad	42 μrad	0.17 mrad	53 μrad
50 μm slit	0.48 mrad		0.18 mrad	73 μrad

crystal plane and calculate the energy. The exact Bragg angle should be corrected by the deviation due to refraction by about 6 μrad, which corresponds to a correction in energy of about 0.06 eV for Si(404) at 9.1 keV. On the third graph of Fig. 8, in both (404) and ($\bar{4}$04) profiles, a dip exactly at the center is observed and this could be due to multiple diffraction with (800) planes in back diffraction (Nikulin *et al.*, 2003). The same Si(404) profile, with the dip, due to multiple diffraction, is reported by Chang *et al.* (1998) in the GIXD (grazing-incidence X-ray diffraction) geometry.

The line of triangles at the top of each graph in Fig. 8 is the transmitted beam recorded by the second ionization chamber (IC2, Fig. 6). The increase in intensity is due to anomalous transmission and the reduction of intensity is due to anomalous absorption. Kishino (1971) and Kishino *et al.* (1972) showed that there is an enhancement of the anomalous transmission in the case of extremely asymmetric diffraction.

The energy chosen for the experiments was 9131.55 eV, corresponding exactly to $\theta_B = 45^\circ$ for Si(404).

The energy of the X-ray beam, with this method, is calibrated with an accuracy of about 0.1 eV at 10 keV.

A device to calibrate energy can be realized by knowing the angle between two crystal planes of the same family. Only a well defined energy will satisfy the Bragg diffraction condition in both Bragg planes simultaneously, as explained above. A high-resolution goniometer is necessary for positioning the crystal at the beam and to do the necessary θ scan, but high precision is not required. Indeed, the goniometer need not be an absolute or accurate goniometer. For the tilt (rotation around z axis) angular correction, it was possible to use a rough goniometer because a tilt error of 4.8 mrad leads to a correction in θ_B of only 5.8 μrad, $\Delta E \sim 0.06$ eV.

4. Characterization of the three peaks

To find the properties of the three diffracted beams, a crystal analyzer and a slit were used. The 2θ arm was positioned (see insert in Fig. 9, position A) on the beam that goes through the sample at the diffraction condition. The crystal analyzer, configured in an antiparallel (dispersive, $+n$, $+m$) arrangement with the beamline Si(111) sagital monochromator, was rotated (θ-analyzer scan) to analyze the direct beam. The θ-analyzer scan on Fig. 9 shows a dip that corresponds to the wavelength that is being diffracted by the crystal sample.

The θ-analyzer scan with Si(440) in the direct beam results in a FWHM of about 0.35 mrad, corresponding to a divergence of the incoming beam of 63 μrad and energy spread of 2.5 eV (Fig. 9). When the reflection of the Si(220) analyzer was chosen, an energy spread of 2.3 eV was obtained. Using a 50 μm slit, the observed energy spread was 3 eV. A summary of the results is in Table 1 in the column headed 'Direct', which adds the deconvoluted results for Si (220) and the 50 μm slit. That is, the divergence of the incident beam is around 60 μrad.

The crystal analyzer was positioned at the dip (position -46.835°) on the top of the curve and a 2θ scan (see insert of Fig. 9 at position B) was performed, with the result displayed in Fig. 7. Xc is the center of the peak obtained by a Gaussian fit.

Three set-ups were used to analyze the beam diffracted from the Si(404) sample, two using a crystal analyzer in a parallel arrangement and one using the 50 μm slit. A summary of results is given in Table 1.

The results of a 2θ scan with the Si(440) analyzer (in non-dispersive, $+n$, $-n$ arrangement) shows that the Laue and Bragg diffracted beam widths are of the same order as the width obtained with the 2θ scan of an Si(220) analyzer (in a dispersive, $+n$, $-m$ arrangement). The Si(440) analyzer was in a slightly dispersive set-up with the Si(404) sample because the first crystal (the sample) is diffracting very asymmetrically and the second crystal (the analyzer) is diffracting symmetrically. The central peak, 2θ near 90°, is non-dispersive with respect to the analyzer, and has FWHM of 25 μrad when rocking the sample (θ scan) and FWHM of about 20 μrad when rocking the analyzer (θ-analyzer scan). The theoretical symmetric Si(440) non-dispersive double-crystal rocking curve has FWHM of 15 μrad.

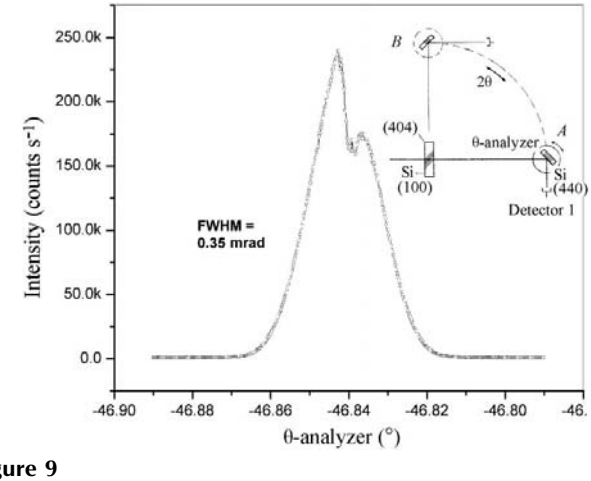

Figure 9
Scan with the crystal analyzer, θ-analyzer scan, Si(440) in anti-parallel set-up, of the transmitted beam through the sample that is in diffraction condition at 9131.6 eV.

The results of a 2θ scan with an Si(220) analyzer for the central peak (2θ near 90°) is about 42 μrad and is bigger than the 20 μrad measured with Si(440) because now the set-up is dispersive and the divergence and chromaticity of the diffracted beam is also being analyzed.

In order to eliminate sensitivity to the chromaticity of the diffracted beam, 2θ scans were done with a 50 μm slit positioned at 0.85 and 0.28 m from the sample. By doing measurements at two distances, we can separate the effects of size and divergence of the diffracted beam being analyzed.

Measuring the width of the peaks at 0.28 and 0.85 m and deconvoluting from the slit width, assuming a Gaussian shape, gives, for the Laue peak, a divergence of about 0.49 mrad and a spatial size of about 20 μm. For the Bragg peak, the procedure yields a divergence of about 0.18 mrad and a size of about 21 μm. The angular widths of both peaks are in agreement with results obtained using the Si(440) and Si(220) crystal analyzers. The FWHM of peak 2 (center) is dominated by the size of the slit. That is, the 50 μm slit is not appropriate to analyze the narrow peak 2.

The geometry using asymmetric Si(404) diffraction with the beam normal to the (100) surface coincides with a multiple diffraction (404 with $\bar{4}04$ and 800) case (Pacherová, 1994) and the extra beam, which comes from the side face, could be a result of multiple diffraction. To verify this, an Si{311} diffraction family plane was chosen to confirm that the extra beam (peak 2 in Fig. 7) is an effect due to the extremely asymmetric diffraction case and not to multiple diffraction. The measurements were done using a conventional X-ray source with Cu target. The $K\beta$ line wavelength diffracted by the Si(311) corresponds to an emerging beam grazing the Si(100) surface. Fig. 10 shows the diffracted beam recorded by a direct conversion X-ray CCD camera. The horizontal displacement corresponds to the 2θ angular displacement. On the third image from the top, one can see the three diffracted beams.

In the case where the incident beam is wider than the crystal thickness, the crystal will concentrate the incoming beam in one direction, the z size of the incident beam will be compressed by the thickness of the crystal (Fig. 6), and beam number 2 in Fig. 7. The same principle could be used to inject X-rays in waveguides.

5. Miscut error

It is important to know the miscut error, the error in the angle that the diffracting crystal plane forms with the crystal surface (angle α in Fig. 2) because the diffraction occurs in a way that the beam emerges grazing the surface and a few mrad of miscut error is enough to change the calculated corrections by more than 20%. The angle α can be determined knowing the position of the θ axis for a Bragg diffraction (θ goniometer calibration) and the energy that was diffracting, by the procedure already described in §3 and determining the position of the crystal surface by means of the total reflection of X-rays on the surface. The measured angle between the surface and the (100) crystal plane was about 314 ± 35 μrad ($0.018 \pm 0.002°$) for the actual sample orientation. For Si(404), α is equal to 785.71 mrad (44.982°) and results in ψ'^{L}_{hB} equal to 314 μrad.

6. Theoretical corrections

Using equations (2) and (3) and $\theta_B = 45°$ for the 404 reflection, $\chi_0 = -5.55 \times 10^{-6}$, $\psi'^{L}_{hB} = -314$ μrad for the Bragg case resulting in a correction of $\Delta\theta_{hc} = 2.06$ mrad. For the Laue case, $\psi'^{L}_{hB} = 0$ (due to the miscut error, a Laue-case diffracted beam is not expected, and for this reason the Laue-case calculation is carried out assuming no miscut error) and results in a correction of $\Delta\theta_{hc} = -2.36$ mrad. The sum of the calculated angles above, $\Delta\theta_{hc}(\text{Bragg}) + \psi'^{L}_{hB} + \Delta\theta_{hc}(\text{Laue})$, is equal to 4.73 mrad and is 75% of the measured angular distance from the Laue peak to the Bragg peak (Fig. 7: $90.21 - 89.85 = 0.36°$, 6.28 mrad). The disagreement between theory and experiment may be caused by errors in the measurement of

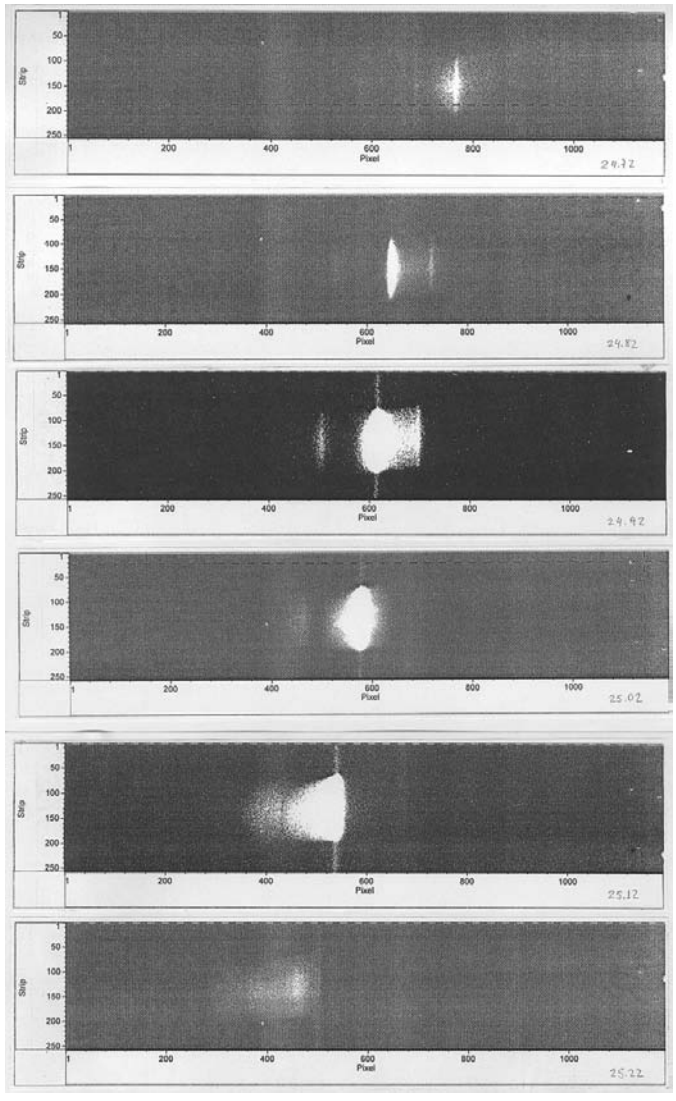

Figure 10
Image of the extremely asymmetric diffracted beam at different θ angles (24.72 to 25.22°, from top to bottom) in 0.1° step^{-1}. Si(311) and Cu $K\beta$ radiation was used.

the miscut angle and/or an inaccuracy in the measurement of the incident energy. Any parameter that can change the grazing angle of the diffracted beam will have a strong influence on the calculated $\Delta\theta_{hc}$.

Using equation (4) and $\theta_B = 45^\circ$ (404 reflection at 9131.5 eV), $\chi_0 = -5.55 \times 10^{-6}$, $2\delta_o = 10.6$ µrad, $\psi'^{L}_{hB} = -314$ µrad, the result for $2\delta_{hc}$ is 79 µrad (FWHM) for the Bragg-case diffracted profile. It is smaller than the measured value of 0.2 mrad and most of this difference can be explained by the divergence and chromaticity of the incident beam.

The origin of the beam that emerges from the side face of the crystal can be explained by the graphical model in Fig. 11.

The incident wavevector, $K_o^{(a)} = \overline{OM}$, excites a wavefield inside the crystal and two wavefields are generated in the direction of the side face, S_1 from tie point P_1 on branch 1 and S_2 from tie point P_2 on branch 2. At the lateral interface (crystal to vacuum), the combination of these two wavefields, $K_{h1}^{(d)} = \overline{HN_1}$ from P_1 and $K_{h2}^{(d)} = \overline{HN_2}$ from P_2, will generate a diffracted beam with angular direction near to the normal of the lateral face.

A theoretical analysis on diffraction in the extremely asymmetric case was done by Bedynska (1973) and predicts a phenomenon of total *internal* reflection of the diffracted waves. This could explain some of the properties of the lateral emerging beam.

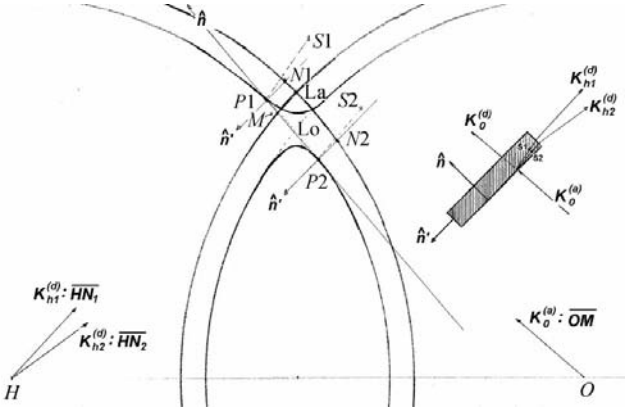

Figure 11
Dispersion surface for the case of a beam emerging from the lateral face, perpendicular to the entrance face.

7. Conclusions

An unusual case has been shown of X-rays diffracted in an extremely asymmetric geometry that leads to three diffracted beams, two of them expected from the extended dynamical theory and an extra one reported here and explained by a dispersion-surface diagram. The three diffracted beams effect was observed in both (404) and (311) crystal planes of a silicon slab with a [100] surface direction and is not an effect of multiple diffraction. The divergence of 20 µrad for the extra beam (the beam emerging from the lateral face) was much smaller than the measured divergence of the two other beams.

The authors are grateful to Dr Guinter Kellermann and Dr Carlos M. Giles A. de Mayolo for helping at the XD2 beamline; to Dr Fabio Furlan Ferreira and Wilson de Carvalho Junior for helping at the XPD beamline; and to Marcelo G. Hönnicke and Dr Irineu Mazzaro for valuable discussions. EMK gratefully acknowledges a scholarship from CNPq/GD. This work has been supported by the Brazilian Synchrotron Light Source (LNLS) under proposal D10A-XRD2-2359 & 2041, by PRONEX/CNPq and PRONEX/F. Araucária.

References

Authier, A. (2001). *Dynamical Theory of X-ray Diffraction*, ch. 8, and references listed therein. Oxford University Press.
Basile, G., Bergamin, A., Cavagnero, G., Mana, G., Vittone, E. & Zosi, G. (1995). *IEEE Trans. Instrum. Meas.* **44**, 526–529.
Bedynska, T. (1973). *Phys. Status Solidi A*, **19**, 365–372.
Bedynska, T. (1974). *Phys. Status Solidi A*, **25**, 405–411.
Chang, S. L., Huang, Y. S., Chao, C. H., Tang, M. T. & Stetsko, Y. P. (1998). *Phys. Rev. Lett.* **80**, 301–304.
Giles, C., Yokaichiya, F., Kycia, S. W., Sampaio, L. C., Ardiles-Saravia, D. C., Franco, M. K. K. & Neuenschwander, R. T. (2003). *J. Synchrotron Rad.* **10**, 430–434.
Gramotnev, D. K. (1997). *J. Phys. D Appl.Phys.* **30**, 2056–2062.
Härtwig, J. (1981). *Acta Cryst.* A**37**, 802–804.
Kishino, S. (1971) *J. Phys. Soc. Jpn*, **31**, 1168–1173.
Kishino, S., Noda, A. & Kohra, K. (1972). *J. Phys. Soc. Jpn*, **33**, 158–166.
Mohr, P. J. & Taylor, B. N. (2000). *Rev. Mod. Phys.* **72**, 351–495.
Nikulin, A. Y., Souvorov, A., Goodden, K., Tamasaku, K. & Ishikawa, T. (2003). *J. Phys. D Appl. Phys.* **36**, A87–A92.
Pacherová, O. (1994). *Acta Cryst.* A**50**, 220–224.